Supplementary Information (SI)

High-Energy Ball Milling-Driven La/Zr Doping of Magnetic Na-A Zeolite Derived from Coal Gangue for Efficient Phosphate Removal

Xiangwu Meng, [a, b, c] Jianjun Li, [d] * Liangji Xu, [c] Changguo Xue, [d] Xuekai Wang, [d] Linlin Song [d]

[a] *State Key Laboratory Mine Response and Disaster Prevention and Control in Deep Coal Mine, Anhui University of Science and Technology, Huainan 232001, China.*

[b]*School of Earth and Environment, Anhui University of Science and Technology, Huainan, 232001, China.*

[c]*Institute of Energy, Hefei Comprehensive National Science Center, Hefei 230000, China.*

[d*]*School of Materials Science and Engineering, Anhui University of Science and Technology, Huainan, 232001, China.*

** Prof. Jianjun Li, Email: lijj3@aust.edu.cn*

List of Supporting Information (SI)

2. Experimental

2.1 Materials and Chemicals

The Si and Al content of raw materials plays an important role in the crystallization process of zeolites (**Fig. S1**). In this experiment, the CG (Coal Gangue) used has a relatively high SiO_2 content and a lower Al_2O_3 content. Na-A zeolite ($Na_{96}Al_{96}Si_{96}O_{384}\cdot 216H_2O$) has a higher Al content. To adjust the Si and Al content in the raw material, $NaAlO_2$ was added as an aluminum source to the ICG.

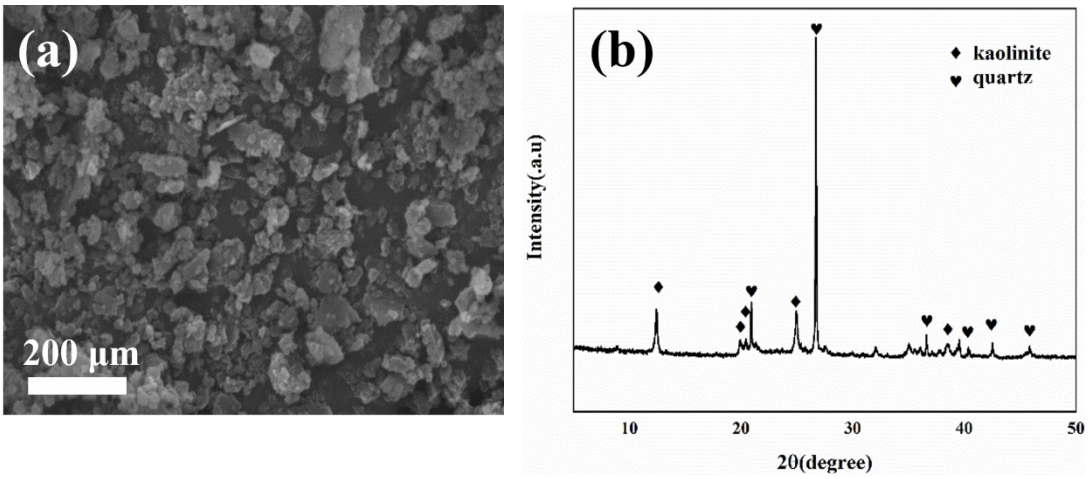

Fig. S1 XRD and SEM pattern of coal gangue.

Table. S1 Typical chemical composition of coal gangue in China.

Area / Elements	SiO_2	Al_2O_3	CaO	Fe_2O_3	Na_2O	MgO	TiO_2	K_2O	SO_3	Loss
Yu Lin	60.38	24.73	0.81	5.76	0.89	1.37	1.36	4.31	0.11	/
Bao Tou	39.08	31.06	0.38	1.20	0.16	0.24	0.98	/	/	26.60
Fang Shan	49.41	21.3	2.52	6.02	1.44	1.56	0.94	2.85	0.65	12.75
Bei Jing	49.90	24.41	0.82	6.42	1.46	1.59	0.88	2.06	0.12	11.76
Shan Dong	48.82	19.03	2.03	4.47	1.43	2.29	/	0.19	/	16.78
Yi Chang	49.03	34.18	0.20	0.73	/	/	1.72	0.12	0.23	13.50
Peng Xiang	52.56	16.57	1.24	3.35	0.21	2.01	/	2.39	/	20.71

Interpretation: Table S1 was adapted from Ref. (42) (Y. Zhang and T. C. Ling, Constr. Build. Mater., 2020, 234, 117424) to support the measured elemental composition of CG presented in Table 1.

3. Results and discussion

3.1 Characterization of adsorbents

Investigation of Na-A Zeolite Synthesis

As shown in **Fig. S2**, the hydrothermally synthesized Na-A zeolite exhibited a regular cubic morphology. During the synthesis of Na-A zeolite, the addition of an appropriate amount of NaOH promoted the formation of Na-A zeolite while suppressing the generation of Na-X zeolite. As illustrated in **Fig. S2a**, when the OH^- concentration was low, although a large amount of Na-A zeolite had already formed, the particle size distribution was highly non-uniform and a small amount of Na-X zeolite was also observed. With a gradual increase in OH^- concentration, the zeolite particles became more uniform in size and their average particle size decreased accordingly (**Fig. S2bcd**). When the NaOH dosage reached 2.5 g, the average particle size decreased to its minimum value, approximately 1 μm. Under otherwise identical conditions, reducing the crystallization time further produced Na-A zeolite crystals with sizes below 1 μm.

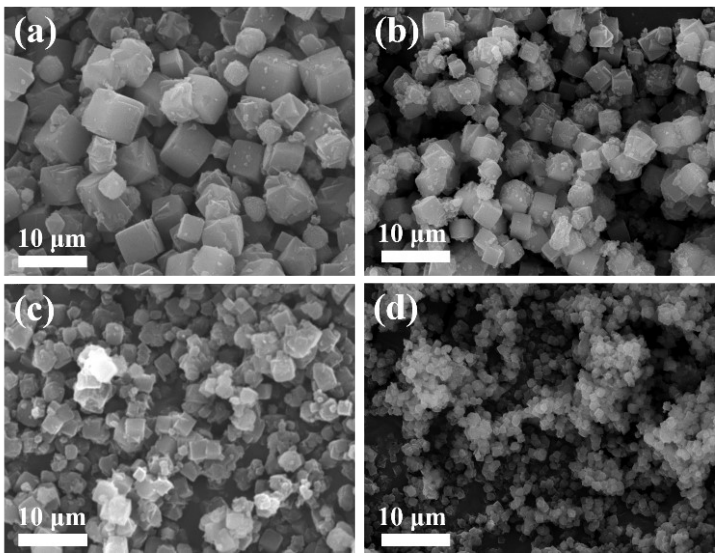

Fig. S2 SEM image of Na-A Zeolite (a) 1.0 g NaOH+9h, (b) 2.0 g NaOH+9h, (c) 2.5 g NaOH+9h, (d) 2.5 g NaOH+6h.

XRD Analysis (**Fig. S3**), the major diffraction peaks of all samples match those of Na-A zeolite (PDF#39-0222), appearing at 2θ = 7.178° (200), 10.158° (220), 12.450° (222), 16.093° (420), 17.642° (422), 20.399° (440), 21.341° (531), and 21.647° (600), confirming the successful formation of Na-A zeolite. The results indicate that the addition of 1 g $NaAlO_2$ promotes the crystallization of Na-A zeolite. Increasing the OH^- concentration further facilitates zeolite crystallization and suppresses the formation of impurity peaks.

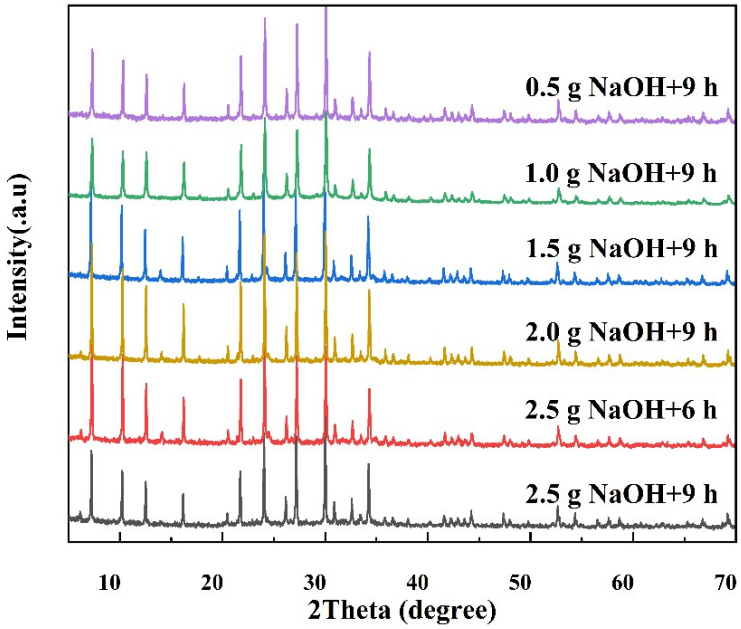

Fig. S3 XRD pattern of Na-A zeolite with prepared different addition amount of $NaAlO_2$.

Adsorption-Desorption Analysis

The physical properties of Na-A zeolites synthesized under different conditions are summarized in **Table. S2**, while the pore-size distribution curves and N_2 adsorption–desorption isotherms are shown in **Fig. 4ab**. As listed in Table S4, the Langmuir specific surface areas of the Na-A zeolites were 5.36, 24.31, and 32.17 m^2/g, respectively, and the corresponding total pore volumes were 0.0167, 0.0578, and 0.0873 cm^3/g. Combined with the observations in **Fig. S2**, these results indicate that the specific surface area increased as the zeolite crystal size decreased. As shown in **Fig. 4a**, most pores were distributed in the range of 2–50 nm, with relatively few pores outside this interval, indicating that the increase in OH^- concentration promoted the development of pore volume. The N_2 adsorption–desorption isotherms (**Fig. 4b**) exhibited H3-type hysteresis loops with no obvious saturation adsorption plateau.

Table. S2 Physical properties of Na-A zeolite.

Sample	Specific surface area (m^2/g)	Average pore size (nm)	Total pore volume (cm^3/g)	Micropore volume (cm^3/g)	Mesopore volume (cm^3/g)
2.0 g+9 h	5.36	18.14	0.0167	0.0006	0.0161
2.5 g+9 h	24.31	12.89	0.0578	0.0067	0.0511
2.5 g+6 h	32.17	15.06	0.0873	0.0079	0.0794

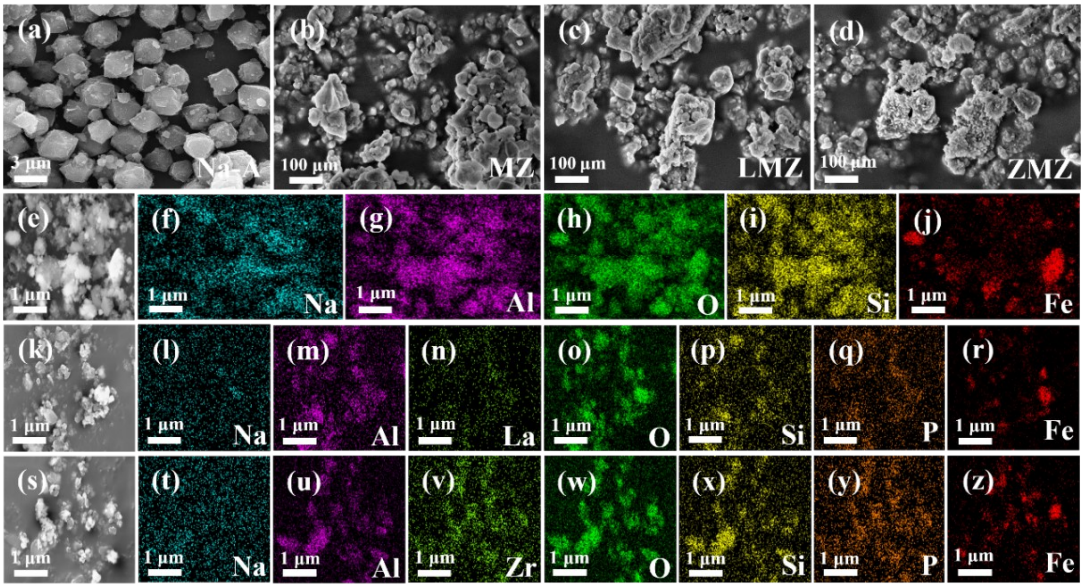

Fig. S4 SEM image of (a-d) Na-A zeolite, MZ, LMZ, ZMZ;

EDS image of MZ (e-j), LMZ (k-r), ZMZ (s-z) elemental mapping.

Structural analysis of different MZ samples

As shown in **Fig. S5a**, Fe_3O_4 displays characteristic reflections at 2θ = 18.3°, 30.1°, 35.4°, 37.1°, 43.1°, 47.1°, 53.4°, 56.9°, and 62.5°, indexed to the (111), (220), (311), (222), (400), (331), (422), (511), and (440) planes, respectively. Pristine Na-A zeolite shows only the Na-A phase. MZ-3, MZ-4, and MZ-5 retain the reflections of both Fe_3O_4 and Na-A, indicating that the zeolite framework is largely preserved after compositing, although the weakened Na-A peaks suggest reduced crystallinity after ball milling. In contrast, no Na-A reflections are observed for MZ-1 and MZ-2, implying substantial structural damage at higher Fe_3O_4 loading.

As shown in **Fig. S5b**, all samples exhibit typical S-shaped hysteresis loops. At an Fe_3O_4: Na-A mass ratio of 1:4, the sample shows an M_s of 17.38 emu g^{-1} and an M_r of 1.68 emu g^{-1}, which is sufficient for rapid magnetic separation. With increasing Fe_3O_4 content, M_s increases from 18.38 to 41.95 emu g^{-1} as the Fe_3O_4: Na-A ratio rises from 1:4 to 1:1. Considering both phase preservation and magnetic separability, MZ-4 was selected for subsequent studies.

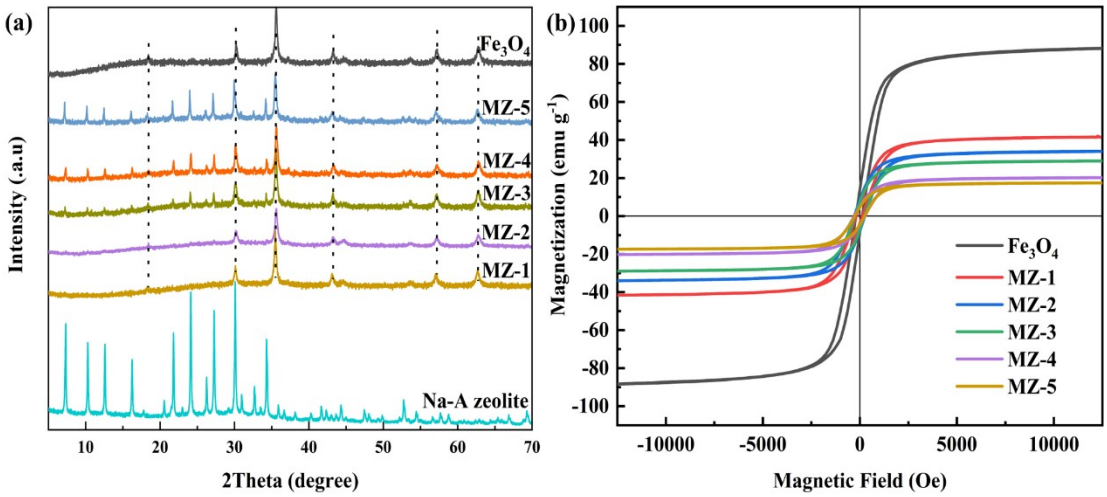

Fig. S5 XRD image of (a) Fe_3O_4, MZ ((a) NO. 1-5)) and VSM image of (b) Fe_3O_4, MZ ((a) NO. 1-5)).

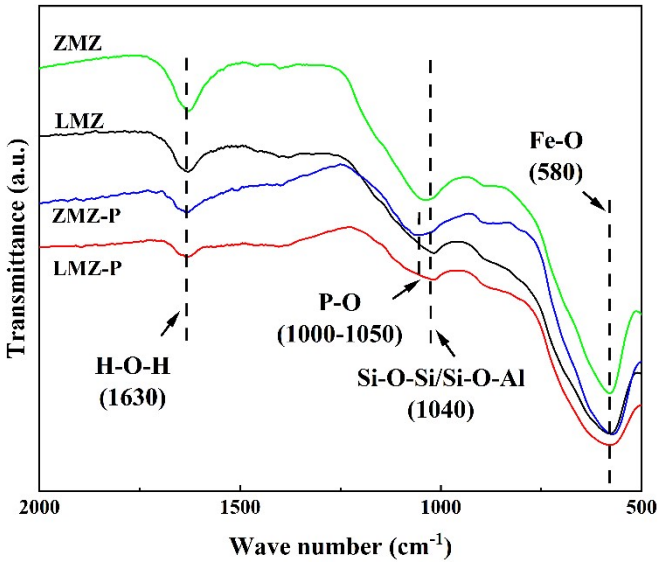

Fig. S6 FT-IR spectra of LMZ, LMZ-P, ZMZ, and ZMZ-P before and after phosphate adsorption.

Effect of coexisting ions on phosphate adsorption

To evaluate the anti-interference performance of LMZ and ZMZ under more complex water-chemistry conditions, phosphate adsorption was examined in the presence of Cl^-, NO_3^-, SO_4^{2-}, HCO_3^-, CO_3^{2-}, Ca^{2+}, and Mg^{2+}. The blank control showed negligible phosphate loss, confirming that phosphate removal mainly resulted from adsorption by LMZ and ZMZ. Without competing ions, LMZ and ZMZ showed adsorption capacities of 26.45 and 22.37 mg P g^{-1}, respectively. Cl^- and NO_3^- caused only slight decreases, whereas SO_4^{2-} showed moderate inhibition. HCO_3^- and CO_3^{2-} produced the strongest suppression, reducing the capacities of LMZ to 21.35 and 18.80 mg P g^{-1} and those of ZMZ to 17.50 and 15.20 mg P g^{-1}, respectively, probably because carbonate species compete for La/Zr coordination sites and buffer the acidic adsorption environment. Ca^{2+} and Mg^{2+} had relatively limited effects. Overall, LMZ maintained higher adsorption capacity than ZMZ under all tested ion conditions, indicating stronger phosphate affinity and better tolerance to coexisting ions.

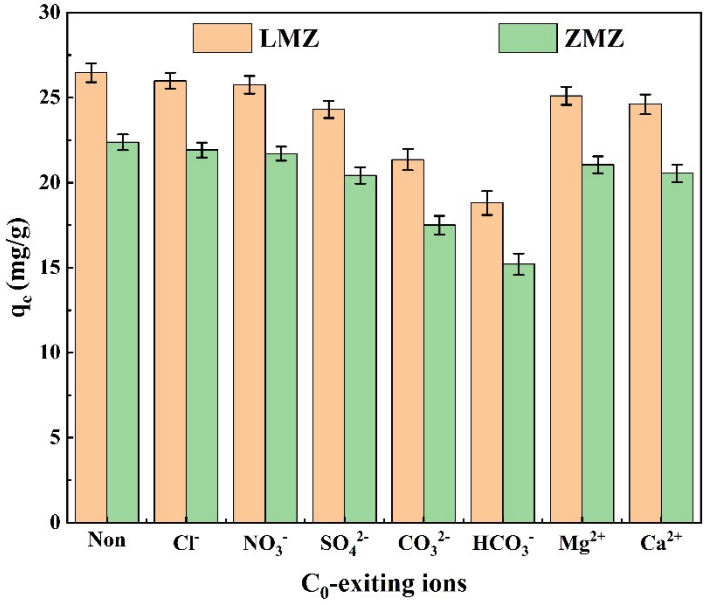

Fig. S7 Influence of different coexisting ions on the adsorption of Phosphate by LMZ and ZMZ.(To evaluate the influence of common coexisting ions, 1 g L^{-1} LMZ or ZMZ was added to 20 mL phosphate solution containing 30 mg P L^{-1} phosphate and selected ions, including Cl^-, NO_3^-, SO_4^{2-}, HCO_3^-, CO_3^{2-}, Ca^{2+}, and Mg^{2+}, at pH 3.0. The suspensions were shaken at 25 °C for 180 min. A blank system without adsorbent was used as the control)

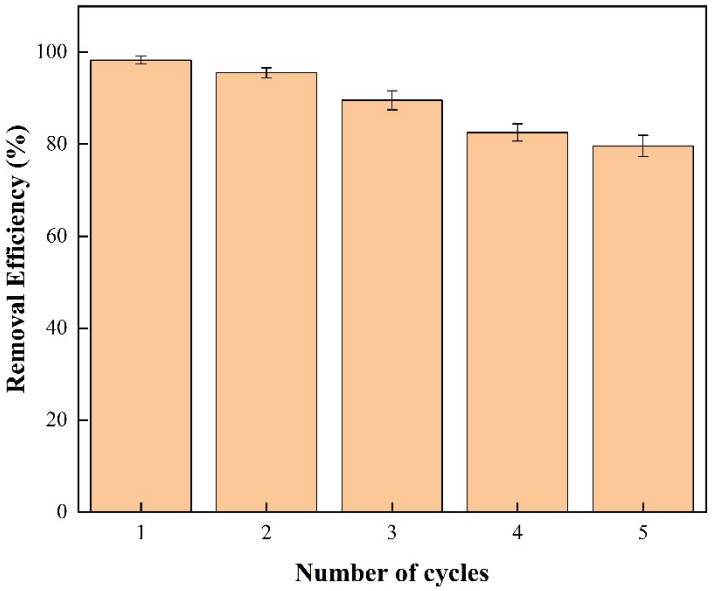

Fig. S8 Cycling performance of LMZ for phosphate removal.

ICP-OES analysis

ICP-OES analysis was further used to quantify the Fe and La/Zr contents in LMZ and ZMZ before and after phosphate adsorption. LMZ contained 14.48 wt% Fe and 40.77 wt% La before adsorption, while ZMZ contained 14.13 wt% Fe and 35.67 wt% Zr, confirming the successful incorporation of abundant La/Zr species into the magnetic zeolite composites. After phosphate uptake, LMZ retained 77.8% of Fe and 69.5% of La, whereas ZMZ retained 78.1% of Fe and 67.1% of Zr. These results provide quantitative compositional evidence for La/Zr incorporation and indicate that a substantial fraction of the magnetic component and La/Zr active sites remained after adsorption, although partial loss of exposed active sites may occur during adsorption and separation.

Thermodynamic analysis

Table. S3 Raw ICP-OES data used for calculation (mg/L).

Sample	Element	Digested mass (g)	Final volume (mL)	Dilution factor	ICP reading	Content (mg g^{-1})	Mass fraction (wt%)	retention (%)
LMZ	Fe	0.0105	25	50	1.216	144.76	14.48	-
LMZ-P	Fe	0.0106	25	50	0.954	112.64	11.26	77.8
LMZ	La	0.0105	25	50	3.425	407.73	40.77	-
LMZ-P	La	0.0106	25	50	2.412	283.25	28.33	69.5
ZMZ	Fe	0.0104	25	50	1.184	141.34	14.13	-
ZMZ-P	Fe	0.0105	25	50	0.927	110.35	11.04	78.1
ZMZ	Zr	0.0104	25	50	2.964	356.73	35.67	-
ZMZ-P	Zr	0.0105	25	50	2.018	239.28	23.93	67.1

Notes: ICP-OES quantification of Fe and La/Zr in LMZ/ZMZ before and after phosphate uptake. 'ICP reading' is the measured concentration of the diluted digest solution. 'Content (mg g^{-1})' was calculated as ICP reading × dilution factor × final volume / digested mass. Mass fraction (wt%) was derived from mg g^{-1} (1 mg g^{-1} = 0.1 wt%).

Thermodynamic analysis

The thermodynamic parameters were further calculated to clarify the temperature dependence of phosphate adsorption. The ΔG⁰ values for LMZ were −3.22, −3.76, and −4.31 kJ mol⁻¹ at 293, 303, and 313 K, respectively, while those for ZMZ were −2.69, −3.14, and −3.59 kJ mol⁻¹. The negative ΔG⁰ values indicate that phosphate adsorption on both adsorbents is spontaneous under the tested conditions. The increasingly negative ΔG⁰ with temperature suggests that elevated temperature favors phosphate uptake. The positive ΔH⁰ values of LMZ and ZMZ, 12.84 and 10.50 kJ mol⁻¹, respectively, indicate an endothermic process, consistent with the increased Langmuir maximum adsorption capacities at higher temperatures. The positive ΔS⁰ values, 54.80 and 45.00 J mol⁻¹ K⁻¹ for LMZ and ZMZ, respectively, suggest increased randomness at the solid–liquid interface, possibly associated with phosphate dehydration, ligand exchange, and La/Zr–phosphate coordination.

Table. S4 Thermodynamic parameters for phosphate adsorption by LMZ and ZMZ.

Adsorbent	**LMZ**	**ZMZ**	**LMZ**	**ZMZ**	**LMZ**	**ZMZ**	**LMZ**	**ZMZ**
***T* (K)**	$ln K_e^0$		***ΔG⁰* (KJ/mol)**		***ΔH⁰* (KJ/mol)**		***ΔS⁰* (J/mol/K)**	
293	1.32	1.10	-3.22	-2.69				
303	1.49	1.24	-3.76	-3.14	12.84	10.50	54.80	45.00
313	1.66	1.38	-4.31	-3.59				